

Direct Observation of Antimagnons with Inverted Dispersion

Hanchen Wang,^{1,*} Junfeng Hu,^{2,†} Wenjie Song,^{2,†} Artim L. Bassant,^{3,†} Jinlong Wang,^{2,4} Haishen Peng,² Emir Karadža,¹ Paul Noël,⁵ William Legrand,⁶ Richard Schlitz,⁷ Jilei Chen,² Song Liu,² Dapeng Yu,² Jean-Philippe Ansermet,^{8,2} Rembert A. Duine,^{3,9,‡} Pietro Gambardella,^{1,§} and Haiming Yu^{4,2,¶}

¹*Department of Materials, ETH Zurich, Zurich 8093, Switzerland*

²*International Quantum Academy, Shenzhen 518048, China*

³*Institute for Theoretical Physics, Utrecht University, Utrecht 3584CC, The Netherlands*

⁴*Fert Beijing Institute, State Key Laboratory of Spintronics,*

School of Integrated Circuit Science and Engineering, Beihang University, Beijing 100191, China

⁵*Université de Strasbourg, UMR 7504, CNRS, Institut de Physique*

et Chimie des Matériaux de Strasbourg, Strasbourg, 67000, France

⁶*Université Grenoble Alpes, CNRS, Institut Néel, Grenoble 38042, France*

⁷*Department of Physics, University of Konstanz, Konstanz 78457, Germany*

⁸*Institute of Physics, École Polytechnique Fédérale de Lausanne (EPFL), 1015 Lausanne, Switzerland*

⁹*Department of Applied Physics, Eindhoven University of Technology,*

P.O. Box 513, 5600 MB Eindhoven, The Netherlands

(Dated: January 22, 2026)

We report direct spectroscopic evidence of antimagnons, i.e., negative-energy spin waves identified by their signature inverted dispersion with Brillouin light scattering (BLS) spectroscopy. We investigate an ultrathin BiYIG film with a perpendicular magnetized anisotropy that compensates the demagnetizing field. By injecting a spin-orbit torque, the magnetization is driven into auto-oscillation and eventually into a non-equilibrium reversed state above a secondary current threshold ($\sim 1.2 \times 10^7$ A/cm²). The dispersion is measured by wavevector-resolved BLS and exhibits a sharp change from an upward dispersion to a downward one, in agreement with theoretical predictions and micromagnetic simulations. Around the threshold current, we observe the coexistence of conventional magnons and antimagnons. Our work establishes antimagnons with inverted dispersion and is a first step towards exploring novel phenomena and applications due to magnon-antimagnon coupling, such as magnon amplification and magnon-antimagnon entanglement, which are part of the emerging field of antimagnonics.

Magnons, the bosonic quasi-particles corresponding to spin-wave excitations, can transfer spin information in magnetic insulators without charge transport and are therefore promising for next-generation spintronic devices with low-power consumption [1–5]. Conventionally, magnons are coherently excited at resonance using microwave antennas that generate large-amplitude spin waves [6–8]. More recently, pure spin currents injected from adjacent heavy metals have been employed to excite magnons and investigate spin transport in magnetic insulators [9, 10], as well as to drive magnetization dynamics via spin-orbit torques (SOTs) [11, 12]. Spin current injection occurs via the spin Hall effect of the heavy metal, which converts a charge current into a transverse spin current [13]. When the SOT generated by absorption of the spin current from the heavy metal overcomes the intrinsic damping [14] of the magnetic insulator, the system enters a regime of auto-oscillation, where sustained magnon excitation occurs without requiring a microwave driving field [15–19]. Ideally, the magnon intensity can be further enhanced by driving a larger current, but is often constrained by dynamic instabilities [20–22] due to nonlinear magnon scattering [23–25]. Recent developments in the growth of magnetic insulators [26–28] have provided a crucial solution to overcome this obstacle by engineering perpendicular mag-

netic anisotropy (PMA) [29] that compensates the shape anisotropy induced by the demagnetizing field, and enables large-angle circular precession [30]. When the PMA compensates the demagnetizing field, a negative damping torque may drive the magnetic system beyond its equilibrium and eventually towards a dynamically stabilized reversed magnetic state, as predicted by recent theoretical studies [31, 32]. Pioneering experiments observed signatures of this inverted state in confined spin-valve and nano-oscillator systems [33, 34] driven by spin-transfer torque (STT) [14, 35]. Very recently, SOT-driven dynamically stabilized inverted states have been experimentally demonstrated in extended magnetic layers using the magneto-optic Kerr effect in a magnetic insulator [36] and spin-torque ferromagnetic resonance in a thin metal film [37].

In the dynamically stabilized state, the magnetization is aligned against the external magnetic field. Small-amplitude perturbations of the magnetization relax the system towards the equilibrium state, parallel to the external field. These perturbations are referred to as antimagnons [38–40] because exciting them lowers the energy of the magnetic system. Therefore, magnons and antimagnons can be produced or annihilated in pairs at no energy cost. The dispersion of antimagnons is predicted to be distinct from that of conventional magnons, featur-

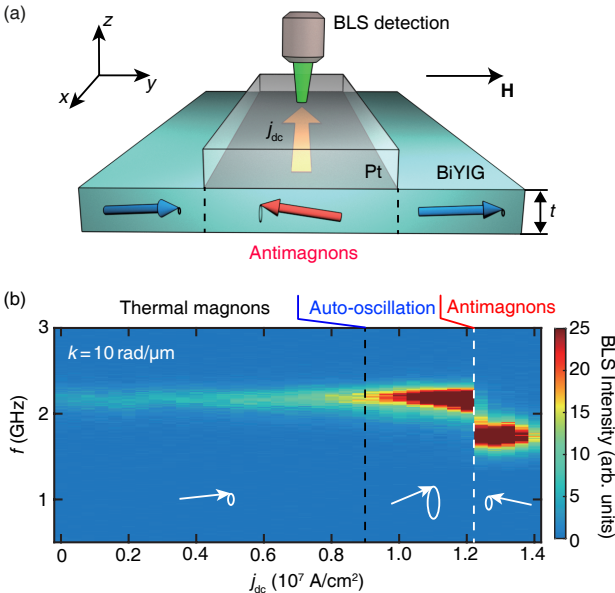


FIG. 1. (a) Schematic illustration of an SOT device based on a BiYIG thin film with a Pt bar on top. The BiYIG film thickness $t = 4$ nm. The Pt bar is about 10 μm wide. A magnetic field of 60 mT is applied along the y direction. An electric direct current (dc) current j_{dc} is applied along the Pt bar and exerts spin-orbit torques on BiYIG underneath to drive its magnetization into auto-oscillation and eventually into a dynamically stabilized non-equilibrium state where antimagnons emerge (red arrow). The Brillouin light scattering (BLS) technique with wavevector (k) resolution is employed to detect magnons. The detection laser spot is placed on the Pt/BiYIG region. (b) BLS spectra measured as a function of current density j_{dc} . The detection wavevector is fixed at $k = 10$ rad/ μm . Three regimes are observed with increasing current density.

ing an inverted curvature with decreasing frequency for increasing wavevectors [31, 38]. Thanks to their inverted dispersion, antimagnons provide unique opportunities to explore novel effects rooted in magnon-antimagnon coupling, such as magnon amplification due to the superradiance [41–44] and magnon entanglement [39–41]. In addition, antimagnons can provide fundamental insight into exotic phenomena such as magnonic Hawking radiation [39, 45–47]. Despite recent theoretical and experimental work, spectroscopic evidence for antimagnons with inverted dispersion remains hitherto elusive.

In this Letter, we report direct observation of antimagnons in a magnetic insulator with inverted dispersion driven by SOT. The key ingredient for the formation of antimagnons is a compensated magnetic system. We fabricated a high-quality 4 nm-thick BiYIG film grown on a (111)-oriented yttrium scandium gallium garnet substrate via high-temperature rf magnetron sputtering [27, 28] [see Supplemental Material (SM) [48] for details]. The PMA is engineered by tuning the tensile strain from the substrate to almost compensate the demagne-

zation field (see SM for ferromagnetic resonance characterization [48]). Subsequently, a 5 nm-thick Pt layer was deposited with dc magnetron sputtering on BiYIG and patterned by e-beam lithography into a 10- μm -wide (along y) and 200- μm -long (along x) bar for SOT injection, as shown in Fig. 1(a) and SM [48]. An electrical dc current of density j_{dc} is applied to the Pt bar (in the $-x$ direction) to exert the SOT on the underlying BiYIG. The antidamping vs damping-like character of the SOT is determined by the relative alignment of the injected spins (polarized along $\pm y$, depending on the sign of j_{dc}) and magnetization. The latter is controlled by an external magnetic field applied along the y direction.

We employ wavevector-resolved Brillouin light scattering (BLS) spectroscopy [50] to study the magnon dispersion of BiYIG capped by Pt. By varying the laser incident angle θ within the xz plane, one can tune the magnitude of the BLS detection wavevector k in the x direction, e.g., $k = 10$ rad/ μm for $\theta = 25^\circ$. Figure 1(b) shows the BLS spectra measured as a function of positive electric current density j_{dc} at $k = 10$ rad/ μm . For a positive current, the SOT has an antidamping character. In the low-current regime, thermal magnons are detected with relatively weak BLS intensity representing the quasi-equilibrium state of the system [9]. As the current density goes above a threshold of about 0.9×10^7 A/cm² [black dashed line in Fig. 1(b)], the BLS intensity rises sharply indicating that the SOT overcomes the intrinsic damping of the system and thus drives the magnetization into auto-oscillation [10, 51–54]. It is noteworthy that auto-oscillation does not occur with negative current even up to -1.4×10^7 A/cm², consistently with the inverted sign of the spin current resulting in a dampinglike torque (see SM for the full spectra [48]).

In conventional in-plane magnetized thin films, the dynamic demagnetizing field compresses the precession trajectory to an elliptical shape, yielding nonlinear magnon scattering that prevents further growth of the precession angle [23–25]. In our PMA-compensated BiYIG film, the auto-oscillation can achieve large-angle circular precession [26, 36]. Interestingly, when j_{dc} further increases over a secondary critical value of $\sim 1.2 \times 10^7$ A/cm² [white dashed line in Fig. 1(a)], an entirely new phase emerges exhibiting an abrupt drop of resonance frequency from approximately 2.2 GHz to 1.7 GHz. This phase corresponds to an inverted magnetization state dynamically stabilized by negative damping [31, 36–38]. By driving even more current in Pt, we find that at $\sim 1.4 \times 10^7$ A/cm² the BLS intensity starts to decrease rather quickly, down to almost the same level of thermal magnons (see SM for the intensity plots [48]). This decrease indicates that, once the magnetization is reversed, further enhancement of the antidamping SOT drives the magnetic system toward increasingly negative temperatures with more spins in the higher-energy antialigned state than in the lower-energy aligned state.

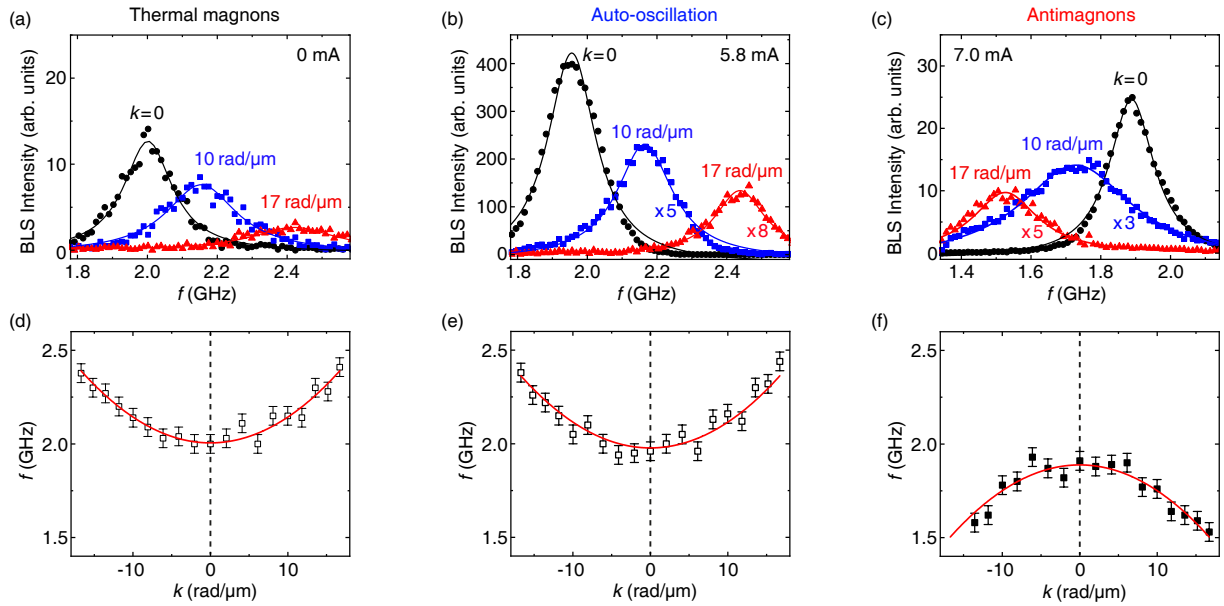


FIG. 2. BLS intensity spectra measured for three different wavevectors (0, 10 and 17 rad/ μm) with (a) zero current, corresponding to thermal magnons, (b) 5.8 mA, corresponding to the auto-oscillation regime, and (c) 7.0 mA, corresponding to the antimagnon regime, where the resonance frequency exhibits a red shift at higher k . The intensity of the high- k spectra in (b) and (c) are amplified for optimized presentation. (d-f) Magnon dispersion relations extracted from a series of BLS spectra in three characteristic regimes of (d) thermal magnons, (e) auto-oscillation and (f) antimagnons. Red solid lines represent the dispersion relations theoretically calculated for the respective cases based on Eq. (1). All data are measured under an applied field of 60 mT.

The collective spin excitations in the inverted magnetic state are called antimagnons [31, 38] and are predicted to exhibit a signature inverted dispersion, in stark contrast with conventional magnons. In order to probe the evolution of the magnon dispersion across the dynamical stabilization threshold, we performed wavevector (k)-resolved BLS measurements at three characteristic current values of $I_{\text{dc}} = 0.0$, 5.8, and 7.0 mA (see SM for BLS methods [48]). Figure 2(a) shows BLS intensity spectra of thermal magnons measured at three different wavevectors of $k = 0$ ($\theta = 0$), 10 rad/ μm ($\theta = 25^\circ$) and 17 rad/ μm ($\theta = 45^\circ$) under an external magnetic field of 60 mT. At higher k , the resonance frequency shifts up as expected for thermal magnons. More BLS spectra at several different wavevectors are shown in the SM [48], from which one can plot the resonance frequency f as a function of k in Fig. 2(d) with $+k$ data extracted from anti-Stokes and $-k$ data from Stokes peaks. The dispersion is fitted with an exchange stiffness $A = 2.8 \text{ pJ/m}$, close to the values reported in previous works [55]. When the current is raised to 5.8 mA [Fig. 2(b)], the system enters auto-oscillation with strongly enhanced BLS intensity. At higher k , the frequency shows again a blue shift. The corresponding dispersion [Fig. 2(e)] remains conventional and can be fitted with an identical curve as that of thermal magnons in Fig. 2(d). Strikingly, when the current rises to 7.0 mA [Fig. 2(c)], the excitation frequency decreases at higher k , i.e., it shows an anomalous

redshift instead of the conventional magnon blueshift reported in Figs. 2(a) and (b). To quantify the dispersion, we extract the peak BLS intensity by performing Lorentz fits to a series of BLS spectra (see SM [48]) and plot the resonance frequency f as a function of the wavevector k . In Fig. 2(f), we clearly observe an inverted dispersion curve which is a hallmark for antimagnons according to theoretical predictions [31, 38].

As antimagnons correspond to linear fluctuations around the non-equilibrium reversed magnetization, their dispersion relation can be derived from the Landau–Lifshitz–Gilbert (LLG) equation [38]. In the limit of negligible dipolar interactions, appropriate for our 4 nm-thick BiYIG film, the dispersion relation simplifies to

$$f(k) = -\frac{\gamma}{2\pi} D k^2 + \Delta, \quad (1)$$

where γ is the gyromagnetic ratio, $D = 2A/M_s$ with A being the exchange stiffness and M_s the saturation magnetization, and Δ represents the frequency of the Kittel mode corresponding to ferromagnetic resonance. The experimental data in Fig. 2(f) are fitted remarkably well using the antimagnon dispersion Eq. (1) with the same exchange stiffness $A = 2.8 \text{ pJ/m}$ and $M_s = 100 \text{ kA/m}$ as required for magnons in Figs. 2(d) and (e). The ferromagnetic resonance frequency $\Delta = 1.89 \text{ GHz}$ is close but not identical to the one measured for magnons at zero current, which we attribute to the effect of Joule

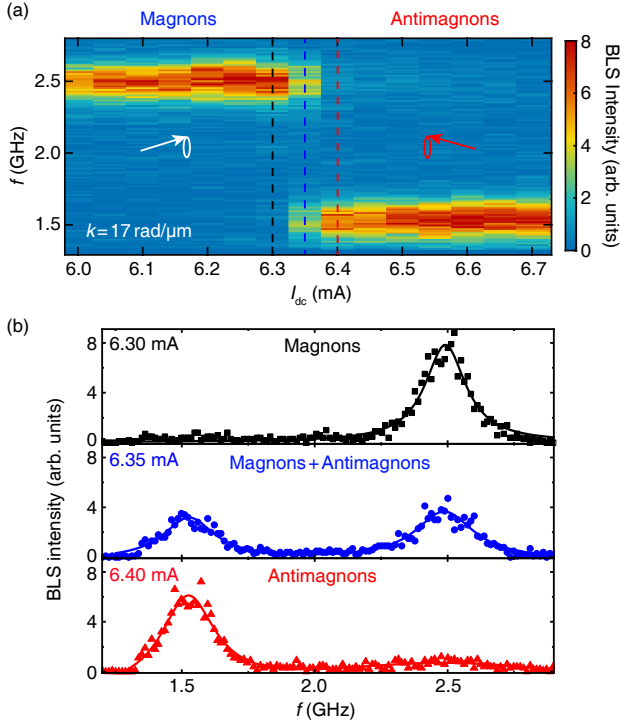


FIG. 3. (a) BLS spectra measured at $k = 17 \text{ rad}/\mu\text{m}$ while sweeping the current I_{dc} from 6.0 to 6.7 mA in increments of 0.05 mA. The external magnetic field is 60 mT. Around 6.35 mA (blue dashed line), the switching from the conventional magnon to antimagnon state occurs accompanied by a sharp change in the resonance frequency. (b) Three representative BLS spectra plotted for $I_{dc} = 6.30$, 6.35 and 6.40 mA around the transition [black, blue and red dashed lines in (a)]. Around 6.35 mA, two peaks are observed indicating the coexistence of the magnon and antimagnon phase.

heating on the magnetization. Thus, the results shown in Fig. 2(f) provide direct evidence for the emergence of antimagnons driven by SOT. Additional characterization of the dispersion under different external magnetic fields, e.g., 40 mT and 70 mT is provided in the SM [48].

From the measured dispersions in Figs. 2(d-f), we learn that the frequency variation between magnon and antimagnon states becomes more pronounced at higher k . Therefore, we push our BLS detection wavevector up to $17 \text{ rad}/\mu\text{m}$ with a laser incident angle around 45° . We then measure the BLS spectra as a function of applied current ranging from 6.0 mA up to 6.7 mA in steps of 0.05 mA, as shown in Fig 3(a). Above the threshold current ~ 6.35 mA, a significant frequency drop of about 1 GHz is detected from ~ 2.5 GHz to ~ 1.5 GHz. In Fig. 3(b), we extract three characteristic BLS spectra around the current threshold. At 6.30 mA, the signal peak centers around 2.5 GHz corresponding to the conventional magnon state, where the magnetization is just about to, but still yet to reverse. Remarkably, at the critical point (~ 6.35 mA) [56], two spectral peaks

emerge, reflecting the coexistence of magnons and antimagnons in critical conditions. This coexistence has not been predicted by theory and is ascribed to the dynamic instability of the system in a chaotic regime [32, 57]. At 6.40 mA, the BLS intensity shifts almost entirely to the low-frequency level at ~ 1.5 GHz, showing that the system has completed the transition into the antimagnon regime following complete reversal of the magnetization.

To further understand the formation of antimagnons and their coexistence with conventional magnons, we perform micromagnetic simulations of the magnetization dynamics using MuMax³ [58] taking into account a dampinglike spin torque [32, 59] to model the spin-wave dispersion across the three different regimes, i.e., thermal magnons, auto-oscillation and antimagnons. The simulated spin-wave dispersions in these regimes show good qualitative agreement with the experimental results presented in Fig. 2. Simulation details and these corresponding spin-wave spectra are provided in the SM [48]. Upon approaching the reversal threshold, the simulated dispersion shown in Fig. 4(a) reveals the simultaneous appearance of both magnon and antimagnon branches. To gain deeper insight into this coexistence, we present a spatial snapshot of the M_y magnetization component taken 75 ns after starting the current, when the system has already reached a steady state dynamics [48]. As shown in Fig. 4(b), the dynamic magnetization texture is spatially inhomogeneous, with some regions pointing along the external field directions and others opposite to it. These regions are populated by magnons and antimagnons, respectively. Notably, for sufficiently large SOT currents, the simulations also show that the magnetization dynamics re-enters a quasi-linear regime in which the magnetization precesses with a small cone angle around the direction opposite to the applied field, in agreement with the decrease of the BLS intensity observed in Fig. 1(b) at

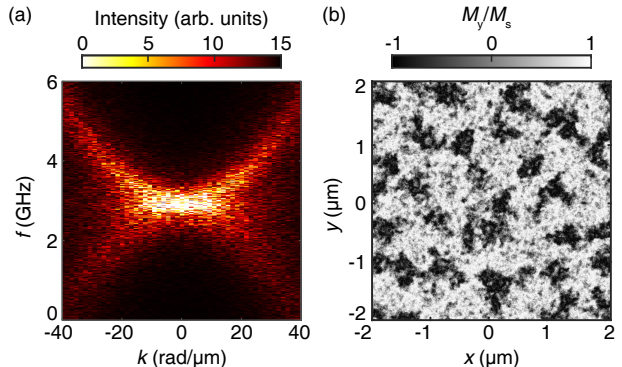


FIG. 4. (a) Magnon dispersion obtained from micromagnetic simulations with a large SOT driving the magnetization at the dynamical stabilization threshold showing the coexistence of magnons and antimagnons in the system. (b) Snapshot of the spatial distribution of the magnetization component M_y at steady state under critical current excitation.

$j_{dc} = 1.4 \times 10^7$ A/cm². The precession is left-handed with respect to the reversed magnetization and right-handed with respect to the applied field, consistent with previous theoretical predictions [31, 38]. This behavior is also in line with our BLS measurements, which show stronger anti-Stokes than Stokes peaks [60] both before and after the magnetization reversal [48].

In summary, we have provided direct experimental evidence for antimagnons with inverted dispersion driven by SOT above a current threshold ($\sim 1.2 \times 10^7$ A/cm²) in a Pt/BiYIG bilayer device. By employing wavevector-resolved BLS spectroscopy, we detect the systematic evolution of magnetization dynamics while continuously raising the antidamping SOT across three successive regimes of thermal magnons, auto-oscillation and antimagnons. The dispersion relations are measured by the BLS and show an abrupt change when the system enters the antimagnonic regime, from a positive curvature for conventional magnons to a fully-inverted downward curvature for antimagnons. This experimental observation is in good agreement with theoretical predictions and is further corroborated by our micromagnetic simulations. At the largest SOT current applied, the system can be dynamically stabilized by the antidamping SOT into a quasi-linear antimagnonic regime. By tuning the SOT precisely to the critical point, we observe the coexistence of both magnons and antimagnons, which provides a unique platform to study novel phenomena related to magnon-antimagnon pair production, such as magnon amplification [42] and magnon-antimagnon entanglement [40, 41]. SOT-driven antimagnons in a fully-compensated magnetic film allow for exploring spin-wave dynamics in non-equilibrium magnetic states beyond traditional spintronic and magnonic systems.

Acknowledgments— We thank I. N. Krivorotov and J. Xiao for helpful discussions. We wish to acknowledge the support by the National Key Research and Development Program of China, Grants No. 2022YFA1402801; NSF China under Grants No. 12525406 and No. 12474104. H.W., E.K., and P.G. acknowledge the support of the Swiss National Science Foundation (Grant No. 200021-236524). H.W. acknowledges the support of the China Scholarship Council (CSC, Grant No. 202206020091). J.H. acknowledges the support from the Shenzhen Science and Technology Program (Grant No. RCBS20231211090814026). A.L.B. and R.A.D. thank the Dutch Research Council (NWO) for funding via the projects “Black holes on a chip” with project number OCENW.KLEIN.502 and “Fluid Spintronics” with project number VI.C.182.069. R.S. acknowledges funding by the Deutsche Forschungsgemeinschaft (DFG, Grant No. 425217212).

* hanchen.wang@mat.ethz.ch; These authors contributed equally to this work.

† These authors contributed equally to this work.

‡ r.a.duine@uu.nl

§ pietro.gambardella@mat.ethz.ch

¶ haiming.yu@buaa.edu.cn

- [1] V. V. Kruglyak, S. O. Demokritov, and D. Grundler, Magnonics, *J. Phys. D: Appl. Phys.* **43**, 260301 (2010).
- [2] A. V. Chumak, V. I. Vasyuchka, A. A. Serga, and B. Hillebrands, Magnon spintronics, *Nat. Phys.* **11**, 453-461 (2015).
- [3] B. Dieny, I. L. Prejbeanu, K. Garello, P. Gambardella, P. Freitas, R. Lehnendorff, W. Raberg, U. Ebels, S. O. Demokritov, J. Åkerman, A. Deac, P. Pirro, C. Adelmann, A. Anane, A. V. Chumak, A. Hirohata, S. Mangin, S. O. Valenzuela, M. Cengiz Onbasli, M. d’Aquinio, G. Prenat, G. Finocchio, L. Lopez-Diaz, R. Chantrell, O. Chubykalo-Fesenko, and P. Bortolotti, Opportunities and challenges for spintronics in the microelectronics industry, *Nat. Electron.* **3**, 446-459 (2020).
- [4] P. Pirro, V. I. Vasyuchka, A. A. Serga, and B. Hillebrands, Advances in coherent magnonics. *Nat. Rev. Mater.* **6**, 1114-1135 (2021).
- [5] H. Y. Yuan, Y. Cao, A. Kamra, R. A. Duine, and P. Yan, Quantum magnonics: When magnon spintronics meets quantum information science. *Phys. Rep.* **965**, 1-74 (2022).
- [6] V. Vlaminck and M. Bailleul, Current-induced spin-wave Doppler shift. *Science* **322**, 410-413 (2008).
- [7] V. E. Demidov M. P. Kostylev K. Rott P. Krzysteczko G. Reiss and S. O. Demokritov, Excitation of microwaveguide modes by a stripe antenna. *Appl. Phys. Lett.* **95**, 112509 (2009).
- [8] H. Yu, O. d’Allivy Kelly, V. Cros, R. Bernard, P. Bortolotti, A. Anane, F. Brandl, R. Huber, I. Stasinopoulos, and D. Grundler, Magnetic thin-film insulator with ultralow spin wave damping for coherent nanomagnonics. *Sci. Rep.* **4**, 6848 (2014).
- [9] L. J. Cornelissen, J. Liu, R. A. Duine, J. Ben Youssef, and B. J. van Wees, Long-distance transport of magnon spin information in a magnetic insulator at room temperature, *Nat. Phys.* **11**, 1022-1026 (2015).
- [10] T. Wimmer, M. Althammer, L. Liensberger, N. Vlietstra, S. Geprägs, M. Weiler, R. Gross, and H. Huebl, Spin transport in a magnetic insulator with zero effective damping, *Phys. Rev. Lett.* **123**, 257201 (2019).
- [11] V. E. Demidov, S. Urazhdin, A. Anane, V. Cros, and S. O. Demokritov, Spin-orbit-torque magnonics, *J. Appl. Phys.* **127**, 170901 (2020).
- [12] A. Manchon, J. Železný, I. M. Miron, T. Jungwirth, J. Sinova, A. Thiaville, K. Garello, and P. Gambardella, Current-induced spin-orbit torques in ferromagnetic and antiferromagnetic systems, *Rev. Mod. Phys.* **91**, 035004 (2019).
- [13] J. Sinova, S. O. Valenzuela, J. Wunderlich, C. H. Back, and T. Jungwirth, Spin Hall effects, *Rev. Mod. Phys.* **87**, 1213-1259 (2015).
- [14] L. Berger, Emission of spin waves by a magnetic multilayer traversed by a current, *Phys. Rev. B* **54**, 9353-9358 (1996).
- [15] M. Collet, X. de Milly, O. d’Allivy Kelly, V. V. Naletov,

- R. Bernard, P. Bortolotti, J. Ben Youssef, V. E. Demidov, S. O. Demokritov, J. L. Prieto, M. Muñoz, V. Cros, A. Anane, G. de Loubens, and O. Klein, Generation of coherent spin-wave modes in yttrium iron garnet microdisks by spin-orbit torque, *Nat. Commun.* **7**, 10377 (2016).
- [16] R. Schlitz, V. E. Demidov, M. Lammel, S. O. Demokritov, and P. Gambardella, Auto-oscillations and directional magnon emission induced by spin current injection into large magnetic volumes, *Nat. Commun.* **16**, 8472 (2025).
- [17] V. E. Demidov, S. Urazhdin, R. Liu, B. Divinskiy, A. Telegin, and S. O. Demokritov, Excitation of coherent propagating spin waves by pure spin currents, *Nat. Commun.* **7**, 10446 (2016).
- [18] T. Chen, R. K. Dumas, A. Eklund, P. K. Muduli, A. Houshang, A. A. Awad, P. Dürrenfeld, B. G. Malm, A. Rusu, and J. Åkerman, Spin-torque and spin-Hall nano-oscillators, *Proc. IEEE* **104**, 1919-1945 (2016).
- [19] E. A. Montoya, X. Pei, and I. N. Krivorotov, Anomalous Hall spin current drives self-generated spin-orbit torque in a ferromagnet, *Nat. Nanotechnol.* **20**, 353-359 (2025).
- [20] H. Suhl, The theory of ferromagnetic resonance at high signal powers, *J. Phys. Chem. Solids* **1**, 209-227 (1957).
- [21] S. M. Rezende, and F. M. de Aguiar, Spin-wave instabilities, auto-oscillations, and chaos in yttrium-iron-garnet, *Proc. IEEE* **78**, 893 (1990).
- [22] I. N. Yemeli, S. Perna, D. Gouéré, A. Kolli, S. Sangiao, J. M. De Teresa, M. Muñoz, A. Anane, M. d'Aquino, H. Merbouche, C. Serpico, and G. de Loubens, Self-Modulation Instability in High Power Ferromagnetic Resonance of BiYIG Nanodisks, *Phys. Rev. Lett.* **135**, 056703 (2025).
- [23] M. Mohseni, Q. Wang, B. Heinz, M. Kewenig, M. Schneider, F. Kohl, B. Lägel, C. Dubs, A. V. Chumak, and P. Pirro, Controlling the Nonlinear Relaxation of Quantized Propagating Magnons in Nanodevices, *Phys. Rev. Lett.* **126**, 097202 (2021).
- [24] L. Sheng, M. Elyasi, J. Chen, W. He, Y. Wang, H. Wang, H. Feng, Y. Zhang, I. Medlej, S. Liu, W. Jiang, X. Han, D. Yu, J.-Ph. Ansermet, G. E. W. Bauer, and H. Yu, Nonlocal Detection of Interlayer Three-Magnon Coupling, *Phys. Rev. Lett.* **130**, 046701 (2023).
- [25] T. Hache, L. Körber, T. Hula, K. Lenz, A. Kákay, O. Hellwig, J. Lindner, J. Fassbender, and H. Schultheiss, Control of Four-Magnon Scattering by Pure Spin Current in a Magnonic Waveguide, *Phys. Rev. Appl.* **20**, 014062 (2024).
- [26] H. Merbouche, B. Divinskiy, D. Gouéré, R. Lebrun, A. El Kanj, V. Cros, P. Bortolotti, A. Anane, S. O. Demokritov, and V. E. Demidov, True amplification of spin waves in magnonic nano-waveguides, *Nat. Commun.* **15**, 1560 (2024).
- [27] W. Legrand, Y. Kemna, S. Schären, H. Wang, D. Petrosyan, L. Siegl, R. Schlitz, M. Lammel, and P. Gambardella, Lattice-tunable substituted iron garnets for low-temperature magnonics, *Adv. Funct. Mater.* **25**03644 (2025).
- [28] H. Wang, W. Legrand, D. Petrosyan, M.-G. Kang, E. Karadža, H. Matsumoto, R. Schlitz, M. Lammel, M.-H. Aguirre, and P. Gambardella, Ultrathin bismuth-yttrium iron garnet films with tunable magnetic anisotropy, *arXiv:2510.07465* (2025).
- [29] L. Soumah, N. Beaulieu, L. Oassym, C. Carrétéro, E. Jacquet, R. Lebourgeois, J. Ben Youssef, P. Bortolotti, V. Cros, and A. Anane, Ultra-low damping insulating magnetic thin films get perpendicular, *Nat. Commun.* **9**, 3355 (2018).
- [30] B. Divinskiy, S. Urazhdin, S. O. Demokritov, and V. E. Demidov, Controlled nonlinear magnetic damping in spin-Hall nano-devices, *Nat. Commun.* **10**, 5211 (2019).
- [31] J. S. Harms, A. Rückriegel, and R. A. Duine, Dynamically stable negative-energy states induced by spin-transfer torques, *Phys. Rev. B* **103**, 144408 (2021).
- [32] H. Ulrichs, From chaotic spin dynamics to noncollinear spin textures in YIG nanofilms by spin-current injection, *Phys. Rev. B* **102**, 174428 (2020).
- [33] B. Özylmaz, A. D. Kent, D. Monsma, J. Z. Sun, M. J. Rooks, and R. H. Koch, Current-Induced Magnetization Reversal in High Magnetic Fields in Co/Cu/Co Nanopillars, *Phys. Rev. Lett.* **91**, 067203 (2003).
- [34] S. M. Mohseni, S. R. Sani, J. Persson, T. N. A. Nguyen, S. Chung, Ye. Pogoryelov, P. K. Muduli, E. Iacobca, A. Eklund, R. K. Dumas, S. Bonetti, A. Deac, M. A. Hoefer, and J. Åkerman, Spin torque-generated magnetic droplet solitons, *Science* **339**, 1295-1298 (2013).
- [35] J. Slonczewski, Current-driven excitation of magnetic multilayers, *J. Magn. Magn. Mater.* **159**, L1-L7 (1996).
- [36] E. Karadza, H. Wang, N. Kercher, P. Noel, W. Legrand, R. Schlitz, and P. Gambardella, Dynamical stabilization of inverted magnetization and antimagnons by spin injection in an extended magnetic system, *arXiv:2601.09569* (2026).
- [37] H. Kurebayashi, J. Barker, T. Yamazaki, V. K. Kushwaha, K. D. Stenning, H. Youel, X. Hou, T. Dion, D. Prestwood, G. E. W. Bauer, K. Yamamoto, and T. Seki, Dynamical stability by spin transfer in nearly isotropic magnets, *arXiv:2601.08738* (2026).
- [38] J. S. Harms, H. Y. Yuan, and R. A. Duine, Antimagnonics, *AIP Adv.* **14**, 025303 (2024).
- [39] T. C. Adorno, S. P. Gavrilov, and D. M. Gitman, Schwinger mechanism of magnon-antimagnon pair production on magnetic field inhomogeneities and the bosonic Klein effect, *Phys. Rev. B* **110**, 014410 (2024).
- [40] E. Kleinherbers, S. P. Kelly, and Y. Tserkovnyak, Entangling color centers via magnon-antimagnon pair creation, *Phys. Rev. Lett.* **134**, 176703 (2025).
- [41] A. L. Bassant, M. E. Regout, J. S. Harms, and R. A. Duine, Entangled magnon-pair generation in a driven synthetic antiferromagnet, *Phys. Rev. B* **110**, 094441 (2024).
- [42] J. S. Harms, H. Y. Yuan, and R. A. Duine, Enhanced magnon spin current using the bosonic Klein paradox, *Phys. Rev. Appl.* **18**, 064026 (2022).
- [43] V. Errani, S. H. Schoenmaker, X. R. Wang, O. Gomonay, and R. A. Duine, Negative-energy spin waves in anti-ferromagnets for spin-current amplification and analogue gravity, *Phys. Rev. B* **112**, 024420 (2025).
- [44] X. R. Wang, X. Gong, and K. Y. Jing, Supermirrors and spin wave amplifications, *Appl. Phys. Lett.* **124**, 082403 (2024).
- [45] A. Roldà-Molina, A. S. Nunez, and R. A. Duine, Magnonic Black Holes, *Phys. Rev. Lett.* **118**, 061301 (2017).
- [46] R. J. Doornenbal, A. Roldà-Molina, A. S. Nunez, and R. A. Duine, Spin-Wave Amplification and Lasing Driven by Inhomogeneous Spin-Transfer Torques, *Phys. Rev. Lett.* **122**, 037203 (2019).

- [47] K. Nakayama, K. Kasahara, T. Inada, and S. Tomita, Spin-Wave Amplification and Lasing Driven by Inhomogeneous Spin-Transfer Torques, *Phys. Rev. Appl.* **22**, 064086 (2024).
- [48] See Supplementary Material for: BiYIG sample growth and characterization, Optical microscope image of the BiYIG/Pt device, BLS spectra measured under damping-like torque, BLS intensity as a function of current density at 10 rad/μm, BLS intensity as a function of current density at 0 rad/μm, Wavevector-resolved BLS measurements, Lorentzian fits of the BLS spectra at different wavevectors, Anti-magnon and thermal magnon dispersions measured under different external magnetic fields, BLS spectra measured at different wavevector, Oersted field generated by the DC current, Simulated time-domain evolution of the magnetization dynamics driven by different currents and the corresponding spin-wave dispersion spectra, Role of magnetization compensation in SOT-driven reversal, and Magnon handedness in magnon and antimagnon phases, which include the Refs. [49].
- [49] W. Legrand, D. Petrosyan, H. Wang, P. Helbingk, R. Schlitz, M. Lammel, J. B. Youssef, and P. Gambardella, Implementation of field-differential phase-resolved microwave magnetic spectroscopy, *Rev. Sci. Instrum.* **96**, 034708 (2025).
- [50] S. O. Demokritov, B. Hillebrands, and A. N. Slavin, Brillouin light scattering studies of confined spin waves: linear and nonlinear confinement, *Phys. Rep.* **348**, 441-489 (2001).
- [51] V. E. Demidov, S. Urazhdin, H. Ulrichs, V. Tiberkevich, A. Slavin, D. Baither, G. Schmitz, and S. O. Demokritov, Magnetic nano-oscillator driven by pure spin current, *Nat. Mater.* **11**, 1028-1031 (2012).
- [52] Z. Duan, A. Smith, L. Yang, B. Youngblood, J. Lindner, V. E. Demidov, S. O. Demokritov, and I. N. Krivorotov, Nanowire spin torque oscillator driven by spin orbit torques, *Nat. Commun.* **5**, 5616 (2014).
- [53] M. Collet, X. de Milly, O. d'Allivy Kelly, V. V. Naletov, R. Bernard, P. Bortolotti, J. Ben Youssef, V. E. Demidov, S. O. Demokritov, J. L. Prieto, M. Muñoz, V. Cros, A. Anane, G. de Loubens, and O. Klein, Spin-wave-mediated mutual synchronization and phase tuning in spin Hall nano-oscillators, *Nat. Commun.* **7**, 10377 (2016).
- [54] A. Kumar, A. K. Chaurasiva, V. H. González, N. Behera, A. Alemán, R. Khymyn, A. A. Awad, and J. Åkerman, Spin-wave-mediated mutual synchronization and phase tuning in spin Hall nano-oscillators, *Nat. Phys.* **21**, 245-252 (2024).
- [55] B. H. Lee, T. Fakhru, C. A. Ross, and G. S. D. Beach, Large Anomalous Frequency Shift in Perpendicular Standing Spin Wave Modes in BiYIG Films Induced by Thin Metallic Overlays, *Phys. Rev. Lett.* **130**, 126703 (2023).
- [56] T. Zhang, C. Wan, and X. Han, Predictive Indicator of Critical Point in Equilibrium and Nonequilibrium Magnetic Systems, *Phys. Rev. Lett.* **135**, 196705 (2025).
- [57] K.-J. Lee, A. Deac, O. Redon, J.-P. Nozières, and B. Dieny, Excitations of incoherent spin-waves due to spin-transfer torque, *Nat. Mater.* **3**, 877-881 (2004).
- [58] A. Vansteenkiste, J. Leliaert, M. Dvornik, M. Helsen, F. Garcia-Sanchez, and B. V. Waeyenberge, The design and verification of MuMax3, *AIP Adv.* **4**, 107133 (2014).
- [59] H. Ulrichs, V. E. Demidov, and S. O. Demokritov, Micromagnetic study of auto-oscillation modes in spin-Hall nano-oscillators, *Appl. Phys. Lett.* **104**, 042407 (2014).
- [60] C. Kim, S. Lee, H.-G. Kim, J.-H. Park, K.-W. Moon, J. Y. Park, J. M. Yuk, K.-J. Lee, B.-G. Park, S. K. Kim, K.-J. Kim, and C. Hwang, Distinct handedness of spin wave across the compensation temperatures of ferrimagnets, *Nat. Mater.* **19**, 980-985 (2020).